Multichannel RRKM-TST and Direct-Dynamics VTST Study of the Reaction of Hydroxyl Radical with Furan

S. Hosein Mousavipour,* Shapour Ramazani, and Zahra Shahkolahi

Department of Chemistry, College of Sciences, Shiraz University, Shiraz 71454, Iran

Received: August 9, 2008; Revised Manuscript Received: January 18, 2009

The kinetics and mechanism of the reaction of OH with furan have been theoretically studied. The potential energy surface for each possible pathway has been investigated by employing DFT, G3MP2, and CCSD methods. The potential energy surface consists of one hydrogen-bonded complex and two energized intermediates. Three different pathways are suggested to be possible for the title reaction. The most probable channel is the hydroxyl radical addition to the C_2 position on the furan ring to cause the ring-opening process. The two other pathways are hydrogen abstraction from one of the C_2 or C_3 position on furan and hydroxyl radical substitution at the C_2 or C_3 position on furan. Abstraction and substitution channels are minor paths at low temperature, but they become comparable with addition channels at high temperature. Addition and substitution reactions proceed via formation of two energized intermediates, Int_1 and Int_2. Multichannel RRKM-TST calculations have been carried out to calculate the individual and overall rate constants for addition and substitution reactions. Direct-dynamics canonical variational transition-state theory calculations with small curvature approximation for tunneling were carried out to study hydrogen abstraction pathways.

Introduction

Furan is a heterocyclic aromatic molecule that is released into the atmosphere by various sources such as combustion of fossil fuels, refuse, plants, and biomass burning.[1] The elementary gas-phase reactions of furan with reactive atoms and radicals are of considerable importance in the atmospheric chemistry and combustion of hydrocarbons. Due to its aromaticity, the behavior of furan is quite different from that of the more typical heterocyclic ethers such as tetrahydrofuran. This molecule is considerably more reactive than benzene in electrophilic substitution reactions. The hydroxyl radical is one of the important oxidizing agents in the chemistry of atmosphere and combustion processes. The hydroxyl radical and ozone are mainly responsible for the gas-phase chemical loss of most organics.[2] Despite some efforts on understanding the kinetics and mechanism of the reaction of OH radical with furan, there are still some uncertainties about the whole mechanism and role of formation of energized intermediates in the kinetics of the title reaction besides the branching ratios. Theoretical studies could be very helpful in understanding the role of potential wells in reactions consisting of multiple channels. To the best of our knowledge, no theoretical study on the kinetics of the title reaction has been reported in the literature.

In this study, the dynamics of reaction of the hydroxyl radical with furan is theoretically investigated. Thus, a thorough study on the mechanism of the OH + furan reaction is reported for the first time, and potential energy surfaces for all possible channels are considered to emphasize their relative importance on kinetics of the system. Three distinct reaction paths exist for the reaction of OH radicals with furan. The major path is the addition of OH radical to furan ring to cause ring-opening channel. The second path is the electrophilic substitution reaction in which OH is substituted for the hydrogen atoms positioned on C_2 or C_3 on the furan ring. The third path is hydrogen abstraction from one of the two positions in the furan ring (C_2 or C_3) to form water and furyl radical. Possible pathways for the reaction of OH with furan are described as follows:

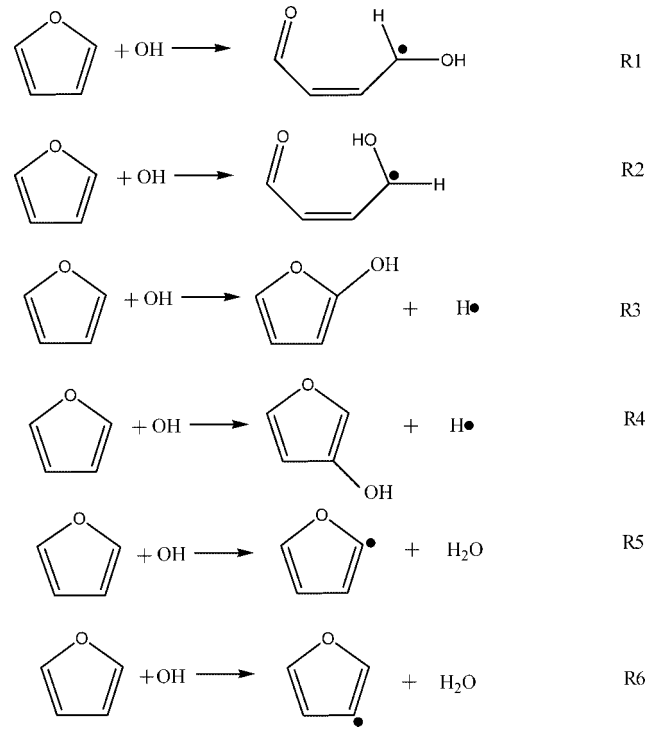

In each of the reactions R1 and R2, electrophilic addition of OH radical to furan causes the ring-opening and the products of the reactions are just different in the spatial position of the OH group.

R3 or R4 is the substitution reaction of OH radical with the hydrogen atom at the C_2 or C_3 position, respectively, on the

* To whom correspondence should be addressed. E-mail: mousavi@susc.ac.ir.

10.1021/jp807122m CCC: $40.75
Published on Web 02/27/2009

furan ring. Reactions R5 and R6 are hydrogen abstraction by OH radical from the furan ring. It is obvious that C_5 and C_4 are equivalent to C_2 and C_3, respectively, and H_9 and H_8 are equivalent to H_6 and H_7, respectively; see Figure 1.

To our knowledge, the only experimental study that represents the major product determination of OH + furan is the work done by Bierbach et al.[3] without reporting any kinetic data. The other previous experimental studies on the kinetics of this system have been carried out by just monitoring the rate of consumption of the reactants without any kinetic analysis of the products.[4−9] Lee and Tang[7] in a resonance fluorescence experiment have studied the reaction of OH radical with furan, ethane, and thiophene at room temperature by monitoring the concentration of OH radicals. Thus, the room temperature rate constant for the reaction of OH with furan was estimated as 6.3×10^{10} L mol^{-1} s^{-1}.

Wine and Thompson[8] in 1984 investigated the kinetics of OH reactions with furan, thiophene, and tetrahydrothiophene over the temperature range of 254−425 K. Hydroxyl radicals were produced by flash photolysis of water vapor at $\lambda > 165$ nm and detected by time-resolved resonance fluorescence spectroscopy. They have found that the reaction of OH with furan is very fast with negative activation energy over the 254−425 K temperature range. The following Arrhenius expression, for the overall rate of consumption of reactants in the OH + furan reaction, is given as $k = 8.0 \times 10^9 \exp(2.8 \text{ kJ mol}^{-1}/RT)$ L mol^{-1} s^{-1}.

In 1991, Grosjean and Williams[9] studied the structure−reactivity and linear free-energy relationships for environmentally important chemical reactions of unsaturated aliphatic contaminants in air and water. They reported a value of 4.0×10^{10} L mol^{-1} s^{-1} for the rate constant of the reaction of hydroxyl radical with furan at room temperature.

Bierbach et al.[10] in 1992 determined the rate constant for the gas-phase reaction of hydroxyl radical with the cyclic ethers such as furan, 2-methylfuran, 2-ethylfuran, and 2,5-dimethylfuran at 300 K in 760 Torr of synthetic air using a relative kinetic technique. They monitored the concentration changes of furan to study the kinetics of reaction of OH + furan. They confirmed the negative activation energy for the latter reaction reported by Wine and Thompson.[8] These authors have concluded that the major pathway in this system is the addition of OH to the C_2 or C_3 position on furan and the attack at the C_2 position is more favorable than that at C_3 position, although the relative importance of the two sites C_2 and C_3 in this reaction was not clear. The total rate constant for the disappearance of the reactants in this system was found to be $(2.5 \pm 0.1) \times 10^{10}$ L mol^{-1} s^{-1}. Bierbach et al. in a Fourier transform infrared (FTIR) absorption spectroscopy study in 1995 have studied the OH-initiated gas-phase oxidation of furan in the presence of synthetic air,[3] and they have been able to monitor consumption of the reactants and formation of the products. They have reported cis/trans-butenedial as the major product for the oxidation of furan in the presence of oxygen at 298 K, which means the major path in this system should be addition of OH radical to furan to cause ring-opening. No kinetic data for the formation of butenedial in the reaction of OH + furan was reported.

Unambiguously, the previous experimental information about the OH + furan reaction is far from satisfactory. In most studies, only the formation of the energized intermediates has been predicted and no kinetic data regarding the formation of possible products are reported, while in ref 3 reaction R1 is reported as the major path with no kinetic data. Therefore, a theoretical study of this important reaction is prompted. It is well-known that ab initio molecular orbital theory plays an important role not only in understanding the overall reaction mechanism but also in interpreting and predicting experimental results. To the best of our knowledge, although two theoretical calculations for the mechanism of reaction of OH + methylfuran,[11] without kinetic data, are reported in the literature, no computational study on the kinetics of the title reaction has been reported to date.

In this Article, we present an extensive theoretical study on the OH + furan reaction. The detailed reaction mechanism is revealed for the first time. The calculations show that the reaction mechanism is much more sophisticated than that expected previously. We used multichannel RRKM and transition-state theory by employing ab initio potential surface data to deduce the rate constants for the addition and substitution channels. Also, direct-dynamics canonical variational transition-state theory calculations with small curvature approximation for tunneling were carried out to study the hydrogen abstraction pathways of the title reaction over the temperature range of 200−3000 K. The present results shed new light on future experiments or dynamical studies.

Computations

Ab initio calculations were carried out using the Gaussian 03 program.[12] The geometries of all the stationary points were optimized at the UMP2,[13] MPWB1K,[14] and G3MP2[15] levels, and single point calculations on the optimized MP2 geometries at the CCSD[16] level along with the 6-31+G(d,p) or 6-311+G(3df,2p) basis set were carried out. The overall energy profiles were explored using the CCSD/6-31+G(d,p)//MP2/6-31+G(d,p) method. The CCSD calculations were performed as full (specifies the inclusion of all electrons in correlation calculations) and also as triple excitations. Harmonic vibrational frequencies were obtained at the MPWB1K/6-31+G(d,p) level in order to characterize stationary points as local minima or first-order saddle points and to obtain zero-point vibration energy corrections. The number of imaginary frequencies (0 or 1) indicates whether a minimum or a transition state has been located. The transition states were subjected to intrinsic reaction coordinate (IRC)[17] calculations to facilitate connection with minima along the reaction paths. Each IRC terminated upon reaching a minimum using the default criterion.

Results and Discussion

Potential Energy Surface and Reaction Mechanism. Optimized geometric structures of the stationary points at the MP2/6-31+g(d,p) level are shown in Figure . The calculated relative energies at different levels of theory and zero-point energies (ZPEs) are listed in Table 1. In Table 1, the results of the CCSD calculations with the 6-31+G(d,P) basis set are compared with the results from the larger basis set 6-311+G(3df,2p) to test the effect of using the larger basis set. Harmonic vibrational frequencies and moments of inertia of the stationary points are listed in Table 2.

A schematic potential energy diagram at the CCSD(full)/6-311+G(3df,2p) is presented in Figure 2. The interaction between the hydrogen atom of the hydroxyl radical and the electron density of the furan π-system forms a prereaction van der Waals complex (vw) in which the hydroxyl radical is almost perpendicular to the furan π-bond with the electron deficient H atom pointing toward the π-system. In the vw complex, the distance of OH from the plane of furan ring is

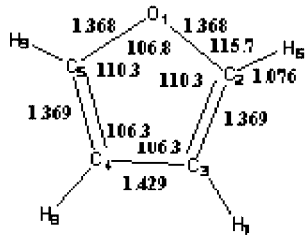

Furan

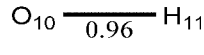

OH

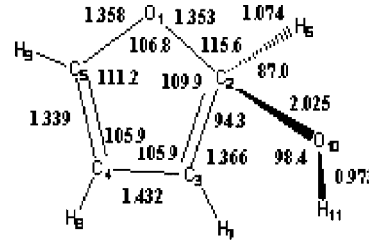

TS_1

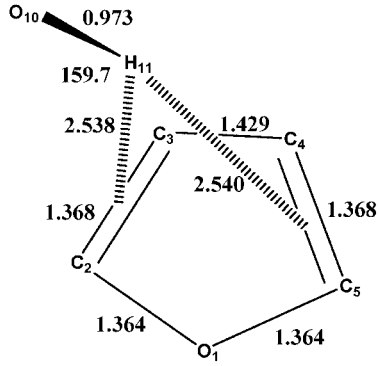

vw

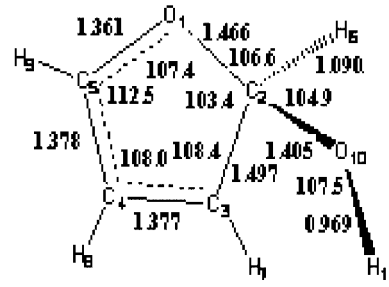

Int_1

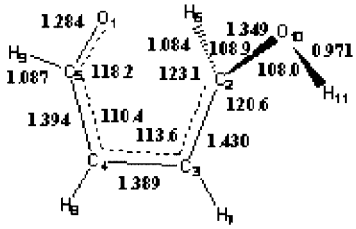

TS_2

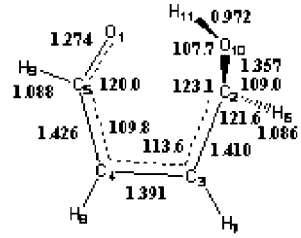

TS_3

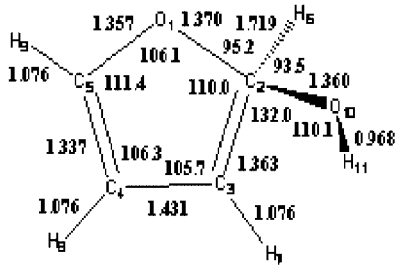

TS_4

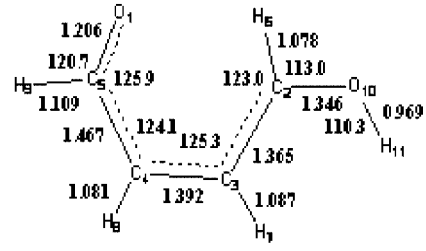

P_1

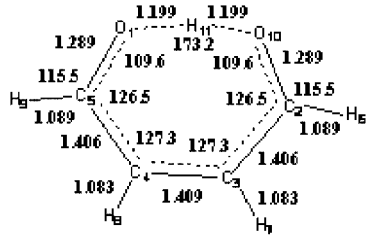

P_2

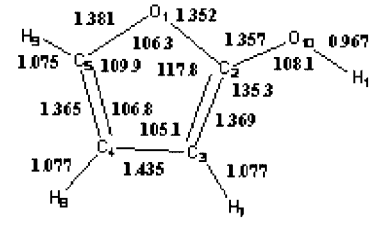

P_3

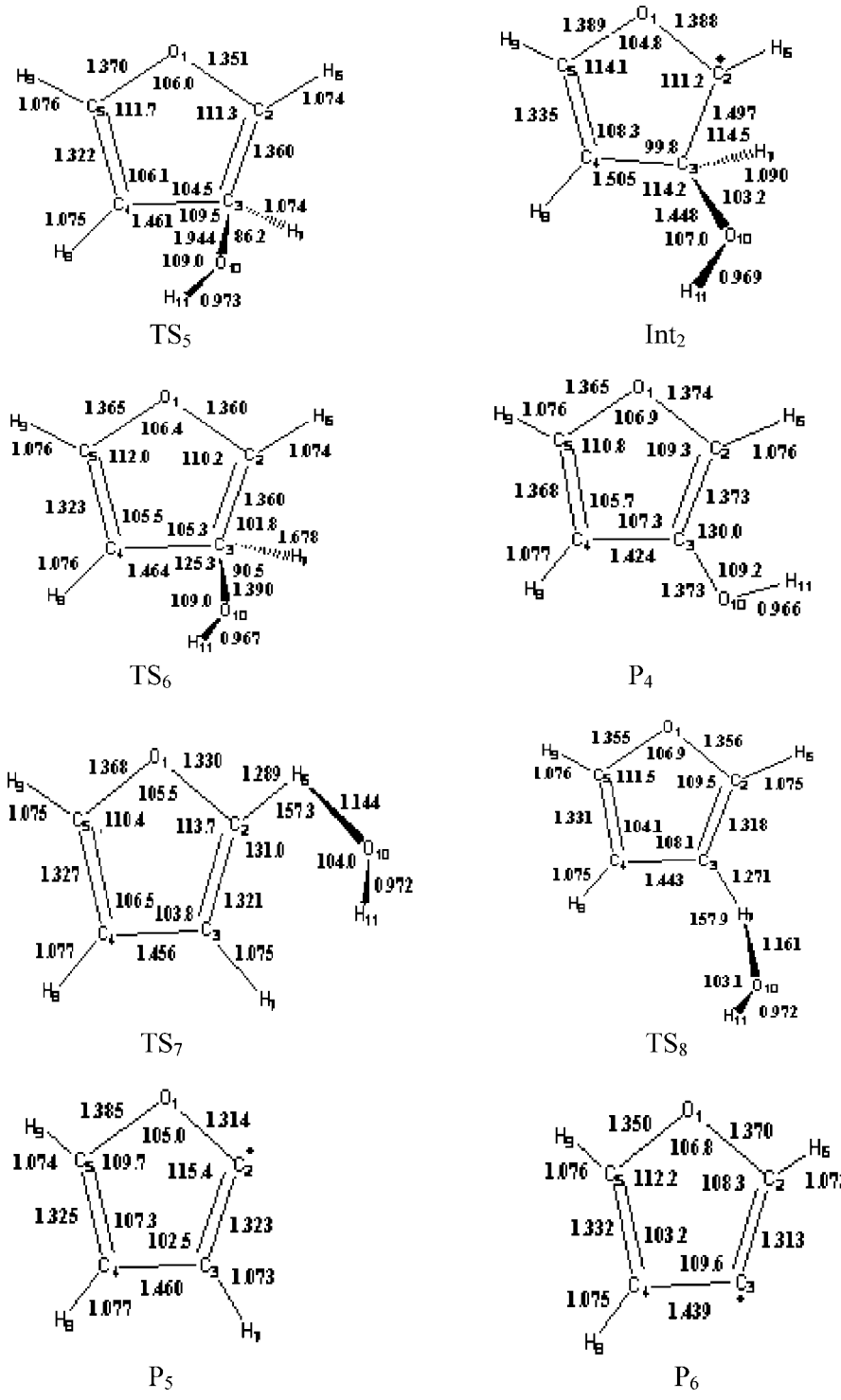

Figure 1. Optimized structure of the stationary points at the MP2/6-31+G(d,p) level.

2.27 Å at the MP2/6-31+G(d,p) level. The stabilization energy of the vw complex changes, depending on the level of theory, from 12.5 to 18.7 kJ mol^{-1} (see Table 1). For addition channels, the oxygen atom of the OH radical should rotate toward one of the carbon atoms on the furan ring. Transition states TS_1 and TS_5 connect the vw complex to the intermediates Int_1 and Int_2, respectively. As shown in Figure 2, the potential energy surfaces for channels R1, R2, and R3 to produce P_1-P_3 products proceed through the formation of energized intermediates Int_1, and that for channel R4 to produce the P_4 product proceeds through the formation of energized intermediate Int_2. Int_1 is 53.0 to −77.4 kJ mol^{-1} more stable than Int_2, depending on the level of calculations, which is due to an additional resonance structure in Int_1 as suggested by Bierbach et al.[10]

Addition of OH radical to the C_2 position on the furan ring produces Int_1 that is followed by C−O bond breaking of the ether (ring) oxygen to produce P_1 or P_2 or substitution channel to produce P_3. As shown in Figure 2, reactions R1 and R2 proceed through two different saddle points TS2 and TS3, respectively, for which their difference is in the spatial orientation of the OH group relative to the plane of the furan

TABLE 1: Relative Energies of Various Species at Different Levels of Theory in kJ mol^{-1} [a]

species	MP_2	CCSD[b]	MPWB1K[b]	0CCSD[c]	G3MP2	ZPE
furan + OH	0.0	0.0	0.0	0.0	0.0	214.4
wv	−18.7	−12.5	−14.8	−15.4 (−17.6)	−13.0	213.4
Int_1	−128.4	−137.4	−155.4	−150.1 (−150.1)	−134.9	233.2
Int_2	−75.4	−66.0	−78.0	−78.2(−79.5)	−60.4	231.8
TS_1	033.6	2.62	−1.3	−5.1 (−14.8)	−8.2	221.0
TS_2	−51.1	−46.5	−64.1	−64.1 (−72.0)	−61.7	224.3
TS_3	−42.7	−20.6	−39.6	−30.5(−47.8)	−39.7	222.8
TS_4	64.4	76.4	33.2	52.5 (43.7)	31.2	211.9
TS_5	48.9	23.8	0.2	24.3 (13.3)	9.7	224.5
TS_6	100.4	109.1	78.8	87.2 (78.6)	68.9	211.3
TS_7	81.9	83.5	52.7	73.5 (63.4)	49.6	209.5
TS_8	74.5	76.6	48.4	67.4 (57.6)	45.8	209.9
P_1	−112.4	−134.8	−150.3	−145.4 (−144.7)	−138.5	224.0
P_2	−187.4	−157.0	−192.9	−168.9(−181.3)	−166.3	226.6
P_3 + H	−14.2	48.5	26.9	29.1 (19.2)	14.9	206.3
P_4 + H	3.4	63.71	45.0	47.4(36.7)	32.1	206.5
P_5 + H_2O	32.9	32.1	21.4	21.6 (20.4)	14.6	215.5
P_6 + H_2O	33.7	30.7	21.2	20.9 (20.1)	14.9	216.5

[a] ZPE calculated at the MPWB1K/6-31+G(d,p) level. [b] Calculated with the 6-31+G(d,p) basis set. [c] Numbers in parentheses are from CCSD(T) calculations.

ring. P_2 was found to be 20.9 kJ mol^{-1} more stable than P_1 at the CCSD(full) level due to the resonance assisted hydrogen bonding as shown below. The barrier for the conversion of P_1 to P_2 was found to be 111.0 kJ mol^{-1}.

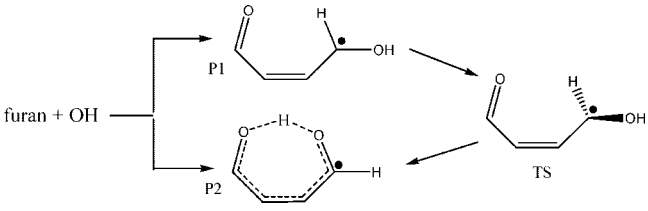

P_3 is 18.5 kJ mol^{-1} more stable than P_4 at the CCSD(full) level, which is due to an additional resonance structure of P_3. The stability of the products of reactions R5 and R6 (P_5 and P_6, respectively) are very close to each other, about 0.4 kJ mol^{-1} at the CCSD(full) level.

The Rate Constants for Different Channels. We have calculated the rate constants for various pathways according to the following simplified mechanism.

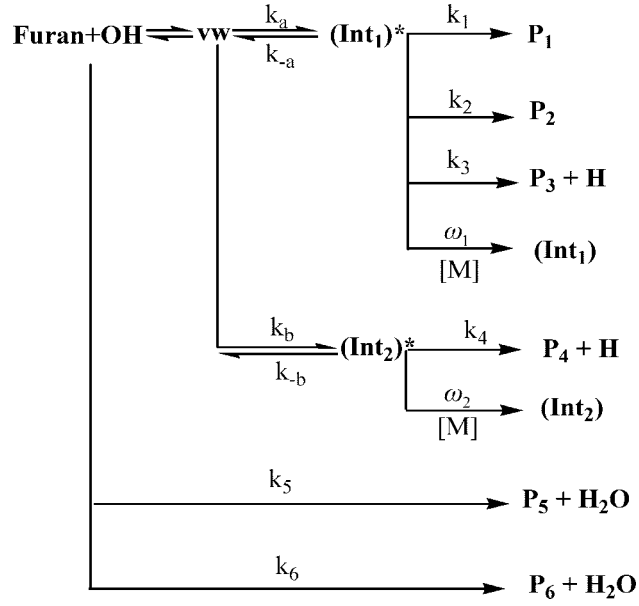

where "*" represents the vibrationally excited intermediates Int_1 and Int_2. ω_1 and ω_2 are the rate constants for the stabilization of these intermediates.

To calculate the individual rate constants for channels R1−R4, we used a RRKM-TST model.[18] We have also calculated the overall rate constants for the consumption of reactants in reactions R1−R3 using a method which combines chemical activation distribution functions and the multichannel RRKM method.[18,19] Steady-state approximation for energized intermediates Int_1 and Int_2 was used to drive the overall rate constant for channels R1−R3 and R4, respectively.

As expected, channels R3−R6 are not important at lower temperatures, but at higher temperatures these channels are expected to become important and competitive with channels R1 and R2. To calculate the rate constants for channels R_5 and R_6, canonical variational transition-state theory, CVT, calculations were performed using POLYRATE9.3.1[20] and GAUSSRATE9.1[21] programs.

As shown in Figure 2, channels R1−R3 and channel R4 proceed through the formation of chemically activated intermediates Int_1 and Int_2, respectively. Steady-state assumption for the energized intermediate Int_1 leads to the following expressions for the second-order rate constants for the formation of P_1, P_2, and P_3 at high pressure limit. It should be noticed that this kind of treatment used to calculate the rate constants is based on a strong collision assumption that causes an overestimation of the rate of collisional stabilization of the intermediates.

$$k_{bi}(P_1) = \frac{\sigma B_e Q^{\#}_{TS1}}{hQ_{furan}Q_{OH}} \exp\left(\frac{-E_0}{RT}\right) \int_0^{\infty} \frac{k_1(\varepsilon)\{G(E_v^+)\} \exp\left(\frac{-E^+}{RT}\right)}{[\omega + k_{-a}(\varepsilon) + k_1(\varepsilon) + k_2(\varepsilon) + k_3(\varepsilon)]} dE^+$$

$$k_{bi}(P_2) = \frac{\sigma B_e Q^{\#}_{TS1}}{hQ_{furan}Q_{OH}} \exp\left(\frac{-E_0}{RT}\right) \int_0^{\infty} \frac{k_2(\varepsilon)\{G(E_v^+)\} \exp\left(\frac{-E^+}{RT}\right)}{[\omega + k_{-a}(\varepsilon) + k_1(\varepsilon) + k_2(\varepsilon) + k_3(\varepsilon)]} dE^+$$

$$k_{bi}(P_3) = \Gamma \frac{\sigma B_e Q^{\#}_{TS1}}{h Q_{furan} Q_{OH}} \exp\left(\frac{-E_0}{RT}\right) \int_0^{\infty} \frac{k_3(\varepsilon)\{G(E_v^+)\} \exp\left(\frac{-E^+}{RT}\right)}{[\omega + k_{-a}(\varepsilon) + k_1(\varepsilon) + k_2(\varepsilon) + k_3(\varepsilon)]} dE^+$$

where Γ is the tunneling factor, σ is the statistical factor (the reaction path degeneracy), $B_e$is the ratio of electronic partition functions, h is Plank's constant, $Q^{\#}_{TS1}$ is the product of translational and rotational partition functions of the transition state for the formation of intermediate Int_1, E_0 is the potential energy barrier for the entrance channel of Int_1 formation, which is corrected for zero-point energy, E^+ is the total nonfixed energy of a given transition state, $G(E_v^+)$ is the sum of vibrational states of the transition state TS_1 at internal energy E_v^+, ω (= $Z\beta_c[A]$) is the collisional stabilization for Int_1, of which β_c is the collision efficiency, and $k_x(\varepsilon)$ is the microcanonical rate coefficient for dissociation of an activated Int_1 in the energy range of ε to $\varepsilon + d\varepsilon$, which is calculated from the quotient of the sum of states to the density of states of the relevant step. The electronic partition function of OH($X^2\Pi$) is $Q_e(OH) = 2 + 2\exp(-200/T)$. We assume no low-lying excited electronic states for the saddle points TS_1 and TS_5.

The tunneling correction factor Γ for steps k_3 and k_4 (C−H bond breaking) was calculated according to a simple expression suggested by Shavitt.[22]

$$Q_{tunnel} = 1 - \frac{1}{24}\left(\frac{h\nu^*}{k_B T}\right)^2 \left(1 + \frac{k_B T}{E_0}\right)$$

where ν^* is the imaginary frequency of the activated complex at the top of the barrier, k_B and h are the Boltzmann and Plank constants, respectively, and E_0 is the barrier height corrected for zero-point energy for the hydrogen transfer steps, k_3 and k_4.

The same method was used to calculate the individual rate for channel R4 according to the above simplified mechanism. According to this method, the following expression was used to calculate the bimolecular rate constant for the formation of P_4.

$$k_{bi}(P_4) = \Gamma \frac{\sigma B_e Q^{\#}_{TS5}}{h Q_{furan} Q_{OH}} \exp\left(\frac{-E_0}{RT}\right) \int_0^{\infty} \frac{k_4(\varepsilon)\{G(E_v^+)\} \exp\left(\frac{-E^+}{RT}\right)}{[w + k_{-b}(\varepsilon) + k_4(\varepsilon)]} dE^+$$

where $Q^{\#}_{TS5}$ is the product of the translational and rotational partition functions of the transition state for the formation of intermediate Int_2 and E_0 is the potential energy barrier for the entrance channel of Int_2 formation, which is corrected for zero-point energy.

To account for the effect of multiple reflections in the vw complex well on the individual rate constants, the probability of the reaction flux passing through each channel was calculated as follows:[23]

TABLE 2: Harmonic Vibrational Frequency (cm^{-1}) and Moments of Inertia (amu $Å^2$) for Various Species at the MPWB1K/6-31+G(d,p) Level

species	frequencies	I_1, I_2, I_3
furan	3357,3352, 3326, 3315, 1625, 1540, 1437, 1312, 1207, 1179 1081, 1078, 1028, 926, 900, 890, 889, 801, 782, 647, 636	105.8, 53.4, 52.4
OH	3978	0.89, 0.89
vw	3819, 3377, 3371, 3350, 3339, 1608, 1538, 1455, 1318, 1267, 1182, 1129, 1091, 1046, 892, 883, 812, 809, 762, 712, 625, 572, 368, 127, 124, 66, 61	184.6, 182.8, 108.4
Int_1	4049, 3422, 3402, 3386, 3214, 1597, 1506, 1468, 1444, 1363, 1318, 1272, 1217, 1158, 1104, 1048, 956, 942, 887, 826, 701, 672, 577, 549, 444, 344, 153	176.6, 130.4, 67.0
Int_2	4056, 3422, 3418, 339, 3186, 1772, 1499, 1461, 1394, 1341, 1311, 1276, 1192, 1143, 1086, 1073, 992, 971, 882, 827, 797, 604, 501, 421, 331, 284, 153	181.9, 138.3, 66.4
TS_1	3904, 3405, 3384, 3367, 3353, 1630, 1555, 1467, 1322, 1282, 1203, 1149, 1101, 1056, 919, 904, 900, 893, 815, 788, 632, 609, 600, 186, 133, 106, 68i	166.0, 164.8, 103.0
TS_2	3930, 3323, 3383, 3275, 3201, 1594, 1559, 1518, 1420, 1366, 1322, 1265, 1156, 1119, 1087, 1044, 950, 868, 825, 694, 612, 576, 547, 467, 343, 189, 453i	209.3, 151.8, 68.2
TS_3	3914, 3320, 3281, 3267, 3186, 1598, 1564, 1504, 1432, 1373, 1332, 1244, 1119, 1109, 1058, 987, 951, 873, 821, 733, 628, 576, 486, 446, 304, 171, 570i	176.7, 127.2, 81.7
TS_4	4029, 3437, 3419, 3402, 1664, 1603, 1505, 1361, 1312, 1296, 1253, 1180, 1086, 1004, 948, 932, 849, 793, 783, 725, 683, 641, 611, 451, 303, 165, 1344i	186.4, 136.7, 58.7
TS_5	4005, 3448, 3438, 3431, 3413, 1697, 1575, 1491, 1353, 1311, 1208, 1157, 1113, 1067, 965, 941, 926, 914, 835, 816, 803, 638, 605, 180, 129, 116, 240i	179.4, 147.9, 75.8
TS_6	4054, 3443, 3435, 3406, 1717, 1640, 1489, 1387, 1327, 1319, 1270, 1164, 1121, 1045, 945, 918, 868, 803, 755, 664, 645, 587, 500, 390, 277, 181, 969i	194.7, 145.7, 58.2
TS_7	3936, 3388, 3374, 3347, 1658, 1554, 1467, 1397, 1284, 1244, 1175, 1124, 1050, 959, 924, 914, 888, 843, 776, 718, 625, 559, 378, 144, 112, 79, 1759i	274.1, 221.4, 54.8
TS_8	3936, 3393, 3384, 3360, 1649, 1580, 1453, 1391, 1285, 1269, 1222, 1129, 1075, 948, 930, 902, 886, 832, 763, 709, 636, 581, 382, 168, 123, 96, 1738i	283.7, 231.3, 54.6
P_1	3943, 3319, 3280, 3215, 3053, 1746, 1647, 1539, 1462, 1416, 1343, 1324, 1208, 1145, 1018, 1004, 979, 913, 848, 373, 531, 519, 414, 323, 195, 193, 173	228.0, 229.1, 58.8
P_2	3291, 3279, 3267, 3130, 2821, 1701, 1679, 1596, 1538, 1499, 1431, 1371, 1242, 1148, 1128, 1020, 973, 961, 939, 904, 726, 656, 544, 318, 306, 302, 152	224.1, 138.0, 86.1
P_3	4104, 3450, 3412, 3399, 1766, 1683, 1587, 1414, 1345, 1269, 1218, 1165, 1080, 1049, 943, 939, 820, 775, 734, 719, 644, 460, 316, 238	100.8, 53.9, 46.9
P_4	4096, 3437, 3430, 3412, 1654, 1787, 1564, 1418, 1355, 1328, 1224, 1153, 1127, 1057, 936, 929, 832, 766, 709, 682, 638, 422, 348, 253	100.4, 53.9, 46.6
H_2O	4014, 3915, 1722	1.75, 1.17, 0.59
P_5	3380, 3376, 3330, 1748, 1635, 1433, 1312, 1234, 1156, 1052, 1026, 978, 916, 900, 862, 828, 638, 591	100.8, 53.9, 46.9
P_6	3387, 3369, 3342, 1739, 1665, 1445, 1319, 1247, 1176, 1090, 1066, 973, 910, 902, 879, 825, 648, 591	100.4, 53.9, 46.6

$$P = \frac{(N_1/N_a)(N_2 + N_3)}{(N_1 + N_2 + N_3) - (N_2 + N_3)(N_1/N_x)}$$

where N_a, N_1, N_2, N_3, and N_x are the sum of states of the reactants, the TS along the reaction path forming the vw complex, TS_1, TS_5, and the complex, respectively. Our calculations revealed that the calculated rate constants for the formation of products P_1 to P_4 decreased by a factor of almost 2.4 because of multiple reflections in the vw complex well at 200 K. At temperatures above 550 K, the presence of the vw complex has no effect on the rate of formation of these products.

The standard RRKM program from Zhu and Hase[24] was used to obtain the sum and density of states. The density of states and sum of states were calculated according to the procedure suggested by Rabinovitch and Whitten,[25] in which only a fraction of the zero-point energy (aE_z) is included in the classical energy at each point along the reaction coordinate. These authors have recommended the following expression to calculate the sum of state:

$$G(E^+) = \frac{(E^+ + aEz)}{s! \prod_{i=1}^{s} h\nu_i}$$

In our RRKM calculations, a step size of $\Delta E^+ = 0.8$ kJ mol^{-1} up to $E^+ = 10.0$ kJ mol^{-1} for lower temperatures, which was increased to a value of 150 kJ mol^{-1} for higher temperatures, was used. N_2 was chosen as bath gas, and a value of 0.5 was selected for the collision efficiency β_c from ref 26.

Temperature dependence of the calculated high pressure rate constants for different channels is shown in Figure 3. The rate constants for reactions R1 and R2 from CCSD/6-31+G(d,p) calculations are also included in the Figure 3 to compare with the results obtained from CCSD/6-311+G(3df,2p). Nonlinear least-squares fitting to the calculated rate constants at the CCSD(full)/6-311+G(3df,2p) level in Figure 3 gave the following expressions for the rate constants of reactions R1−R4.

$$k(P_1) = 1.2 \times 10^{12} T^{-0.55} \exp(-1.7 \text{ kJ}/RT) \text{ L mol}^{-1} \text{ s}^{-1}$$

$$k(P_2) = 5.6 \times 10^{3} T^{1.61} \exp(1.8 \text{ kJ}/RT) \text{ L mol}^{-1} \text{ s}^{-1}$$

$$k(P_3) = 1.83 \times 10^{3} T^{1.43} \exp(-56.8 \text{ kJ}/RT) \text{ L mol}^{-1} \text{ s}^{-1}$$

$$k(P_4) = 1.9 \times 10^{12} T^{-0.87} \exp(-103.8 \text{ kJ}/RT) \text{ L mol}^{-1} \text{ s}^{-1}$$

Nonlinear least-squares fitting to the calculated rate constant R1 at the CCSD/6-31+G(d,p) level gave the following expression.

$$k(P_1) = 2.5 \times 10^{14} T^{-1.62} \exp(-1.8 \text{ kJ}/RT) \text{ L mol}^{-1} \text{ s}^{-1}$$

As shown in Figure 3, reaction R1 is the major path at lower temperatures in this system. Our results indicated that the rate of stabilization of intermediate Int_1 at 760 Torr pressure is negligible relative to the rate of formation of P_1. The stabilization rate for Int_2 is more important than the rate of unimolecular redissociation into the original reactants at temperatures below 500 K, while at higher temperatures the unimolecular redissociation rate becomes more important. At temperatures below 1000 K, the rate of stabilization for Int_2 is more important than the rate of formation of P_4.

Canonical variational transition-state theory was used to calculate the rate constants for channels R5 and R6.

Canonical Variational Transition-State Theory. Canonical variational transition-state theory (CVT)[27] with multidimensional semiclassical transmission coefficients was used to calculate the rate constants for channels R5 and R6. The CVT rate constant, $k^{CVT}(T)$, can be obtained as the minimum of the generalized transition-state theory rate constant, $k^{GT}(T,s)$, at temperature T as a function of reaction coordinate s.

$$k^{CVT}(T) = \min_s k^{GT}(T,S) = \frac{k_B T}{h} \sigma \frac{Q^{GT}(T, s^{CVT})}{Q^R(T)} \exp[-V_{MEP}(s^{CVT})/k_B T]$$

where σ is the symmetry factor (number of equivalent reaction paths), k_B and h are the Boltzmann and Planck constants, respectively, $V_{MEP}(s^{CVT})$ is the classical potential energy along the minimum energy path (MEP) at $s = s^{CVT}$ with the zero of energy at the reactants classical equilibrium position, and $Q^{GT}(T,s^{CVT})$ and Q^R are the quantum mechanical partition functions for the generalized transition state (GTS) at $s = s^{CVT}$ with the zero of energy at $V_{MEP}(s)$ and reactants per unit volume with zero of energy at classical equilibrium, respectively. The

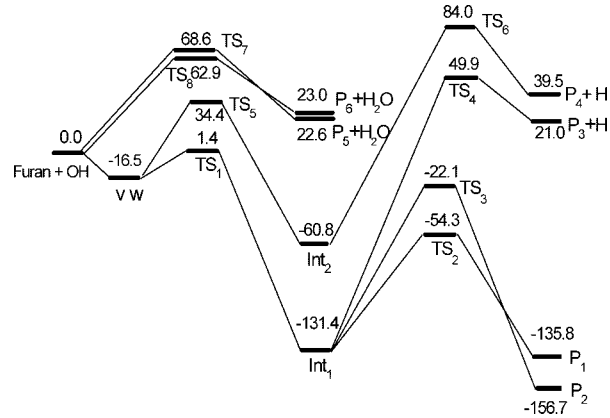

Figure 2. Relative energies of different species in kJ mol^{-1} at the CCSD/6-311+G(3df,2p) level. All values are corrected for zero-point energies.

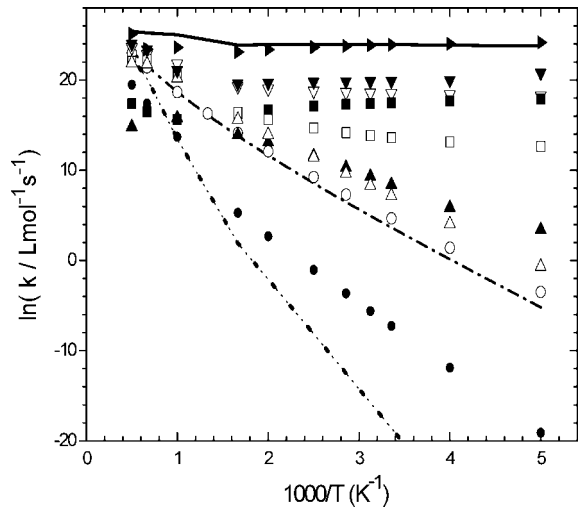

Figure 3. Arrhenius plot of the calculated rate constants for various products at 760 Torr pressure of N_2. Solid line, (▽), (●), and dotted line represent the apparent rate constant for the formation of P_1, P_2, P_3, and P_4, respectively; (■), (▲), (□), and (△) are the rate constants of stabilization and unimolecular decomposition rate constants k_{-a} and k_{-b} of intermediates Int_1 and Int_2, respectively, from CCSD(full)/6-311+G(3df,2p) results. (solid right triangle) and (▼) represent the apparent rate constants for the formation of P_1 and P_2, respectively, from CCSD(full)/6-31+G(d,p) results. Dash-dotted line and (○) are the rate constants for the formation of P_5 and P_6, respectively, from the MPWB1K/6-31+G(d,P) results.

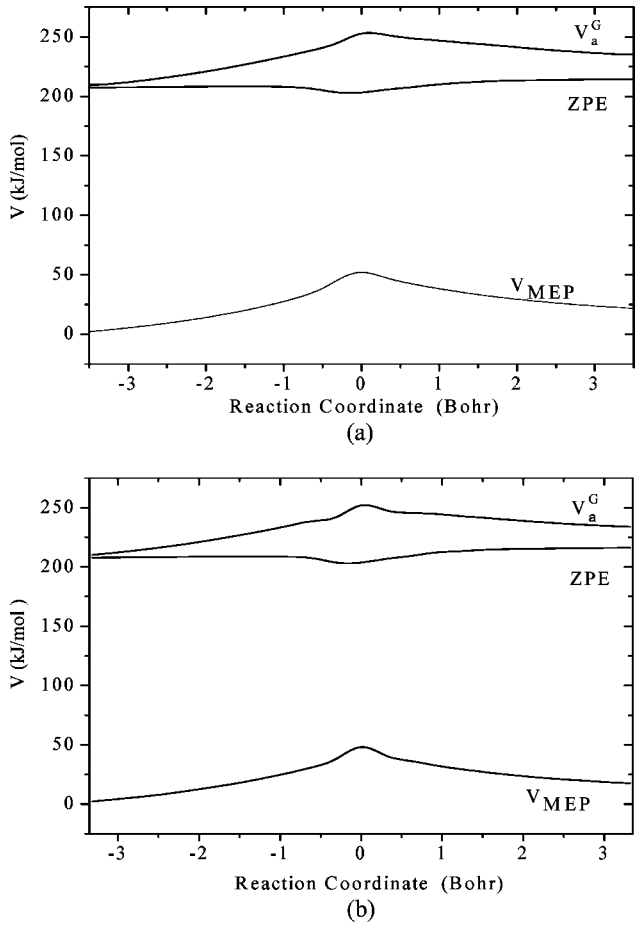

Figure 4. Variation of the vibrationally adiabatic ground-state potential ($V_a^G(s)$), minimum energy path (V_{MEP}), and zero-point energy (ZPE) for reactions R5 (a) and R6 (b).

location of the GTS corresponding to the minimum flux corresponds to a maximum in the generalized standard-state free energy change for the formation of the GTS at s from the reactants.

To incorporate multidimensional quantum effects arising from the motion of the system along the reaction coordinate, the CVT rate constant is multiplied by the ground-state transmission coefficient $\kappa^{CVT/Y}$ (Y is the method for calculating the tunneling factor) that primarily accounts for reaction-path tunneling and nonclassical reflection. The final CVT rate constant is thus given by

$$k^{CVT/Y}(T) = \kappa^{CVT/Y}(T)\, k^{CVT}$$

to account for the dynamical quantum effects of reaction-coordinate tunneling and nonclassical reflection, as well as the nonseparability of such effects from other degrees of freedom.

Small-curvature tunneling (SCT)[28] approximation was used to include the quantum effects in calculating the rate constants for reactions R5 and R6.

CVT Results for Reactions R5 and R6. The minimum energy paths were searched from 4.0 bohr inside the reactants valley up to 4.0 bohr inside the product valley using the step size of 0.02 bohr. The Hessian calculations were performed at 0.2 bohr intervals. Vibrationally adiabatic ground-state potential, $V_a^G(s)$, and minimum energy path potential, V_{MEP}, for reactions R5 and R6 are shown in Figure 4.

In calculating the rate constants for reactions R5 and R6, the motion of the oxygen of the OH radical about the reaction coordinate C—H was treated either as a hindered rotor or a normal vibrational motion. No substantial differences were observed in the results.

Zero and small curvature tunneling approximations were used to calculate the rate constants. Thermally averaged transmission probability, $P(E)\ \exp(-E/RT)$, at several temperatures for reactions R5 and R6 are determined to examine the efficiency of zero curvature tunneling (ZCT) and small curvature tunneling (SCT) approximations. Our results showed that the probability values calculated from SCT approximation are larger than those values calculated by using ZCT approximation.

In Figure 3, the temperature dependence of the rate constants for reactions R5 and R6 are compared with those for the formation of the other products. Nonlinear least-squares fitting to the calculated data in Figure 3 gave the following expressions for the hydrogen transfer rate constants of reactions R5 and R6.

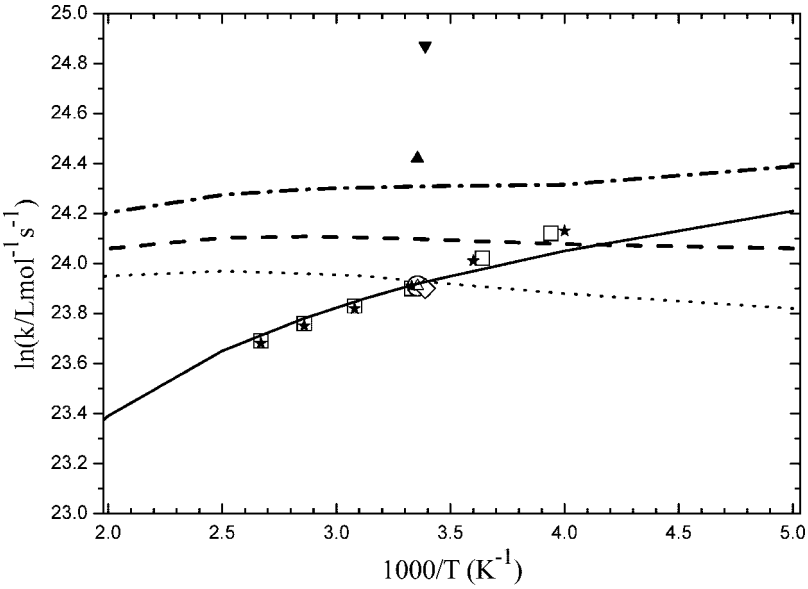

Figure 5. Temperature dependence of the overall rate constant for disappearance of the reactants. Dotted line, dash-dotted line, and dashed line represent the rate constants calculated from the results of the CCSD(full), CCSD(T), and G3MP2 methods, respectively, along with the 6-311+G(3df,2p) basis set. Solid line represents the overall rate constant calculated from the CCSD(full)/6-31+G(d,p) results. Experimental data are shown as (★) from ref 4, (□) from ref 8, (○) from ref 10, (▲) from ref 9, (◇) from ref 5, (△) from ref 2, and (▼) from ref 7.

$$k^{H}(P_5) = 8.3 \times 10^{-1} T^{3.42} \exp(-40.1\ \text{kJ}/RT)\ \text{L mol}^{-1}\ \text{s}^{-1}$$

$$k^{H}(P_6) = 1.1 T^{3.33} \exp(-36.8\ \text{kJ}/RT)\ \text{L mol}^{-1}\ \text{s}^{-1}$$

In Figure 5, we have compared the overall rate of consumption of the reactants at the CCSD(full), CCSD(T), and G3MP2 levels along with the 6-311+G(3df,2p) basis set with reported values in the literature. Our results at the CCSD/6-31+G(d,p) level was also included in Figure 5 and was found to be in good agreement with the reported data in literature. The overall rate constant for the disappearance of the reactants from the CCSD(full)/6-31+G(d,p) level over the temperature range of 200−500 K was found as

$$k_{\text{loss}}(\text{furan}) = 1.9 \times 10^{14} T^{-1.57} \exp(-1.7\ \text{kJ}/RT)\ \text{L mol}^{-1}\ \text{s}^{-1}$$

Conclusions

The thermal rate constants for six different reaction paths in thr OH + furan system were calculated according to our suggested mechanism. Formation of a hydrogen-bonded complex vw with −13.5 kJ mol^{-1} energy relative to total energies of the reactants at the CCSD(full)/6-31+G(d,p) level causes the overall rate constant to decrease by a factor of about 2.4 at 200 K. At temperatures higher than 550 K, this factor reaches a value of about 1.0. The multichannel RRKM-TST method was used to calculate the individual and overall rate constants for those channels that proceed via the formation of the two potential wells. Strong collision assumption was used to calculate the rate constants $k(P_1)$ to $k(P_4)$. Although this kind of assumption caused an overestimation of stabilization rates of intermediates, it did not much affect the rate of the major channel (leading to P_1), as the rate was much higher than that of the overestimated stabilization channel.

CVT calculations were performed to indicate the importance of hydrogen abstraction channels (reactions R5 and R6) in this system.

Channel R1 is the most important channel in this system. The branching ratios for different channels have been predicted for the first time. Although rates of channels R2−R6 are not significant at temperatures lower than 2000 K, it would be good to have an idea about their relative importance. Our results indicate that the stabilization rate of intermediate Int_1 is negligible relative to the rate of formation of P_1 at 760 Torr pressure. Our calculations for the apparent rate constant from the CCSD(full)/6-31+G(d,p) results give the best agreement with the reported experimental data in the literature. The overall rate constant shows negative temperature dependence at temperatures lower than about 600 K. This kind of behavior is due to the formation of two intermediates Int_1 and Int_2. Fast intramolecular vibrational energy redistribution was assumed to calculate the individual rate constants. Good agreement between our results and the reported experimental results indicates that our assumption on treating the vibrations statistically could be reasonable. At temperatures greater than 600 K, the individual rate constants for the formation of P_1 to P_4 show positive temperature dependence. Our results predict that at temperatures above 2000 K the hydrogen abstraction channels become dominant. Unfortunately, no experimental kinetic data above 425 K for this system are available in the literature.

Acknowledgment. The financial support of the Research Council of Shiraz University is acknowledged.

References and Notes

(1) Greenberg, J. P.; Zimmerman, P. R.; Heidt, L.; Pollock, W. J. *Geophys. Res.* **1984**, *89*, 1350. Graedel, T. E.; Hawkins, D. T.; Claxton, L. D. *Atmospheric Chemical Compound: Sources, Occurrence, and Bioassay*; Academic Press: New York, 1986. Khalil, M. A. K.; Rasmussen, R. A. *J. Air Waste Manage. Assoc.* **1992**, *42*, 810. Knudsen, J. T.; Tollstein, L.; Bergstrom, L. *J. Photochem.* **1993**, *33*, 253. Lawrence, M. G.; Jockel, P.; von Kuhlmann, R. *Atmos. Chem. Phys.* **2001**, *1*, 37.

(2) Atkinson, R.; Aschmann, S. M.; Carter, W. P. L. *Int. J. Chem. Kinet.* **1983**, *15*, 51.

(3) Bierbach, A.; Barnes, I.; Becker, K. H. *Atmos. Environ.* **1995**, *29*, 2651. Bierbach, A.; Barnes, I.; Becker, K. H.; Wiesen, E. *Environ. Sci. Technol.* **1994**, *28*, 715.

(4) Atkinson, R. *Chem. Rev.* **1986**, *86*, 69.

(5) Tuazon, E. C.; Atkinson, R; Winerl, A. M.; Pitts, J. N., Jr. *Arch. Environ. Contam. Toxicol.* **1984**, *13*, 691.

(6) Atkinson, R.; Aschmann, S. M.; Carter, W. P. L. *Int. J. Chem. Kinet.* **1983**, *15*, 51.

(7) Lee, J. H.; Tang, I. N. *J. Chem.Phys.* **1982**, *9*, 77.

(8) Wine, P. H.; Thompson, R. J. *Int. J. Chem. Kinet* **1984**, *16*, 867.

(9) Grosjean, D.; Williams, E. L., II *Atoms. Environ.* **1992**, *26A*, 1395.

(10) Bierbach, A.; Barnes, I.; Becker, K. H. *Atoms. Environ.* **1992**, *26A*, 813.

(11) Zhang, W.; Du, B.; Mu, L.; Feng, C. *THEOCHEM* **2008**, *28*, 353. Zhang, W.; Du, B.; Mu, L.; Feng, C. *Int. J. Quantum Chem.* **2008**, *108*, 1232.

(12) Frisch, M. J. ; Trucks, G. W.; Schlegel, H. B.; Scuseria, G. E.; Robb, M. A.; Cheeseman, J. R.; Montgomery, J. A., Jr.; Vreven, T.; Kudin, K. N.; Burant, J. C.; Millam, J. M.; Iyengar, S. S.; Tomasi, J.; Barone, V.; Mennucci, B.; Cossi, M.; Scalmani, G.; Rega, N.; Petersson, G. A.; Nakatsuji, H.; Hada, M.; Ehara, M.; Toyota, K.; Fukuda, R.; Hasegawa, J.; Ishida, M.; Nakajima, T.; Honda, Y.; Kitao, O.; Nakai, H.; Klene, M.; Li, X.; Knox, J. E.; Hratchian, H. P.; Cross, J. B.; Adamo, C.; Jaramillo, J.; Gomperts, R.; Stratmann, R. E.; Yazyev, O.; Austin, A. J.; Cammi, R.; Pomelli, C.; Ochterski, J. W.; Ayala, P. Y.; Morokuma, K.; Voth, G. A.; Salvador, P.; Dannenberg, J. J.; Zakrzewski, G.; Dapprich, S.; Daniels, A. D.; Strain, M. C.; Farkas, O.; Malick, D. K.; Rabuck, A. D.; Raghavachari, K.; Foresman, J. B.; Ortiz, J. V.; Cui, Q.; Baboul, A. G.; Clifford, S.; Cioslowski, J.; Stefanov, B. B.; Liu, G.; Liashenko, A.; Piskorz, P.; Komaromi, I.; Martin, R. L.; Fox, D. J.; Keith, T.; Al-Laham, M. A.; Peng, C. Y.; Nanayakkara, A.; Challacombe, M.; Gill, P. M. W.; Johnson, B.; Chen, W.; Wong, M. W.; Gonzalez, C.; Pople, J. A. *Gaussian 03*, revision B.01; Gaussian Inc.: Pittsburgh, PA, 2003.

(13) Møller, C.; Plesset, M. S. *Phys. Rev.* **1934**, *46*, 618.

(14) Zhao, Y.; Truhlar, D. G. *J. Phys. Chem. A* **2004**, *108*, 6908.

(15) Curtiss, L. A.; Redfern, P. C.; Raghavachari, K.; Rassolov, V.; Pople, J. A. *J. Chem. Phys.* **1999**, *110*, 4703.

(16) Scuseria, G. E.; Schaefer, H. F. *J. Chem. Phys.* **1989**, *90*, 3700. Pople, J. A.; Head-Gordon, M.; Raghavachari, K. *J. Chem. Phys.* **1987**, *87*, 5968.

(17) Gonzales, C.; Schlegel, H. B. *J. Chem. Phys.* **1989**, *90*, 2154. Gonzales, C.; Schlegel, H. B. *J. Phys. Chem.* **1990**, *94*, 5523.

(18) Berman, M. R.; Lin, M. C. *J. Phys. Chem.* **1983**, *87*, 3933. Becker, K. H.; Kurtenbach, R.; Wiesen, P. *J. Phys. Chem.* **1991**, *95*, 2390. Mousavipour, S. H.; Saheb, V. *Bull. Chem. Soc. Jpn.* **2007**, *80*, 1901.

(19) Holbrook, K. A.; Pilling, M. J.; Robertson, S. H. *Unimolecular Reactions*, 2nd ed.; John Wiley & Sons Ltd.: Chichester, England, 1996.

(20) Corchado, J. C.; Chuang, Y.-Y.; Fast, P. L.; Villa, J.; Hu, W.-P.; Liu, Y.-P.; Lynch, G. C.; Nguyen, K. A.; Jackels, C. F.; Melissas, V. S.; Lynch, B. J.; Rossi, I.; Coitino, E. L.; Fernandez Ramos, A.; Pu, J.; Albu, T. V.; Steckler, R.; Garrett, B. C.; Isaacson, A. D.; Truhlar, D. G. *POLYRATE*, version 9.3; Department of Chemistry and Supercomputer Institute, University of Minnesota: Minneapolis, MN, 2003.

(21) Corchado, J. C.; Chuang, Y.-Y.; Coitino, E. L.; Truhlar, D. G. *GAUSSRATE*, version 9.1/P9.1-G03/G98/G94; Department of Chemistry and Supercomputer Institute, University of Minnesota: Minneapolis, MN, 2003.

(22) Shavitt, I. *J. Chem. Phys.* **1959**, *31*, 1359.

(23) Hirschfelder, J. O.; Wigner, E. *J. Chem. Phys.* **1939**, *7*, 616. Miller, W. H. *J. Chem. Phys.* **1976**, *65*, 2216.

(24) Zhu, L.; Hase, W. L. *QCPE Program 644; Quantum Chemistry Program Exchange*; Indiana University: Bloomington, IN, 1993.

(25) Rabinovitch, B. S.; Whitten, G. Z. *J. Chem. Phys.* **1968**, *48*, 1427.

(26) Börjesson, L. E. B.; Nordholm, S. *J. Phys. Chem.* **1995**, *99*, 938.

(27) Garret, B. C.; Truhlar, D. G. *J. Chem. Phys.* **1979**, *70*, 1593. Garret, B. C.; Truhlar, D. G. *J. Phys. Chem.* **1979**, *83*, 1079. Garret, B. C.; Truhlar, D. G. *J. Phys. Chem.* **1979**, *83*, 3058.

(28) Lu, D.-h.; Truong, T. N.; Melissas, V. S.; Lynch, G. C.; Liu, Y.-P.; Garrett, B. C.; Steckler, R.; Isaacson, A. D.; Rai, N. S.; Hancock, G. C.; Lauderdale, J. G.; Joseph, T.; Truhlar, D. G. *Comput. Phys. Commun.* **1992**, *71*, 235.

JP807122M